Time-resolved spectroscopy of the pulsating CV GW Lib

L. van Spaandonk[1]⋆, D. Steeghs[1,2], T.R. Marsh[1], M.A.P. Torres[2]
[1] *Astronomy and Astrophysics, Dept. of Physics, University of Warwick, Coventry CV4 7AL, UK*
[2] *Harvard-Smithsonian for Astrophysics, 60 Garden Street, Cambridge, MA 02138, USA*

arXiv:0909.3991v1 [astro-ph.SR] 22 Sep 2009

ABSTRACT

We present time-resolved optical spectroscopy of the dwarf nova GW Librae during its rare April 2007 super-outburst and compare these with quiescent epochs. The data provide the first opportunity to track the evolution of the principal spectral features. In the early stages of the outburst, the optically thick disc dominates the optical and the line components show clear orbital radial velocity excursions. In the course of several weeks, optically thin regions become more prominent as strong emission lines replace the broad disc absorption.

Post-outburst spectroscopy covering the I-band illustrates the advantages of Ca II relative to the commonly used Balmer lines when attempting to constrain binary parameters. Due to the lower ionisation energy combined with smaller thermal and shear broadening of these lines, a sharp emission component is seen to be moving in between the accretion disc peaks in the Ca II line. No such component is visible in the Balmer lines. We interpret this as an emission component originating on the hitherto unseen mass donor star. This emission component has a mean velocity of $\sim -15 \pm 5$ km s^{-1} which is associated with the systemic velocity γ, and a velocity semi-amplitude of $K_{\rm em} = 82.2 \pm 4.9$ km s^{-1}. Doppler tomography reveals an asymmetric accretion disc, with the S-wave mapping to a sharp spot in the tomogram with a velocity consistent to what is obtained with line profile fitting. A centre of symmetry analysis of the disc component suggests a very small value for the WD orbital velocity K_1 as is also inferred from double Gaussian fits to the spectral lines.

While our conservative dynamical limits place a hard upper limit on the binary mass ratio of $q < 0.23$, we favour a significantly lower value near $q \sim 0.06$. Pulsation modeling suggests a WD mass $\sim 1 M_\odot$. This, paired with a low mass donor, near the empirical sequence of an evolved CV close to the period bounce, appears to be consistent with all the observational constraints to date.

Key words: binaries: spectroscopic – novae, cataclysmic variables – stars: individual: GW Lib

1 INTRODUCTION

Cataclysmic variables (CVs) are semi-detached interacting binary systems containing a white dwarf (WD) primary and a late-type main-sequence secondary (MS) which transfers mass onto the primary through Roche Lobe overflow, see Warner (1995) for a review. Strong and broad emission lines are a common observational feature in the majority of CVs, probing the dissipative processes within the accretion flow. The hydrogen Balmer series usually dominate the spectrum, and in the vast majority of spectroscopic studies of CVs serve as the main proxy for determining the system parameters. However, relatively unexplored spectral features re-

main, such as the Ca II triplet lines in the I-band. Common emission line sources include the accretion disc, the interaction point of the gas stream with the disc (hot spot) and the irradiated face of the secondary star.

GW Lib is a dwarf nova (DN) which was discovered by González & Maze (1983) as it went onto its first recorded outburst and rapidly increased in brightness by 8 magnitudes. It remained in its quiescent state after that period of activity until 2007. Van Zyl et al. (2000) found three periodicities in the quiescent photometric light curve at 236, 376 and 650 s, making the primary in GW Lib the first multi-period non-radial pulsating WD in an accreting binary. Thorstensen et al. (2002) measured the radial velocity curve using Hα and determined a rather short orbital period of 76.79 ± 0.02 min. In the latest Ritter

⋆ E-mail:L.van-Spaandonk@warwick.ac.uk

& Kolb catalogue, only 8 systems with a smaller period are known when excluding the AM CVn systems which have H-deficient donors (Ritter & Kolb 2003), implying an evolved binary close to the period minimum. From model fits to the WD absorption troughs and mean spectra, various temperatures have been found. UV spectra suggest $T_{WD} = 14,700$ K with a WD mass of $0.6M_\odot$ (Szkody et al. 2002) or a dual temperature WD with $T_{low} = 13,300$ K and $T_{high} = 17,000$ K. The latter model can only explain the observed UV/optical pulse amplitude ratio in GW Lib (see table 2 in Szkody et al. 2002) as compared with single pulsating ZZ-Ceti stars, if the WD mass of GW Lib is larger than $0.8M_\odot$. Thorstensen et al. (2002) fit the optical Balmer line profiles to find $T = 13,220$ K and $\log g = 7.4$. However, all temperature estimates place the WD outside the ZZ Ceti instability strip for single WD pulsators. A mass determination based on the detected pulsation periods combined with distance and UV flux constraints suggests a WD mass of $1.02M_\odot$ (Townsley et al. 2004).

On 2007 April 12, amateur astronomers reported the sudden and rapid brightening of GW Lib (Templeton 2007) indicating renewed outburst activity, 24 years after the discovery outburst. The outburst had an amplitude of ~ 9 magnitudes and lasted for several weeks, see Figure 1.

We present the first time-resolved optical spectroscopy of GW Lib in (super)outburst (Section 3) alongside time-resolved optical spectroscopy during quiescence before and after the outburst (Section 4). We present the possible system parameters in Section 5 and the discussion in Section 6.

2   OBSERVATIONS AND REDUCTION

We briefly describe the facilities used below. Full details of the observations can be found in Table 1.

2.1   Telescopes and Instruments

The telescopes used were the Magellan Telescopes operated by the Carnegie Institution of Washington at the Las Campanas Observatory in Chile, the Smithsonian Astrophysical Observatory's Tillinghast Telescope at the Fred Lawrence Whipple Observatory, located on Mount Hopkins near Amado, Arizona and the William Herschel Telescope operated by the Isaac Newton Group on the island of La Palma.

2.1.1   Magellan Telescope

Time-resolved optical spectroscopy was acquired during quiescence with the Baade 6.5-m telescope equipped with the Boller and Chivens Spectrograph (B&C) on 2004 June 6 and 7. The B&C was used with a Marconi 2048×515 CCD with a 13.5 microns pixel size and a 1200 lines mm^{-1} grating covering the spectral interval $3500 - 5100$Å. A slit width of 0.8 arcsec gave a dispersion of 0.79Å pixel^{-1} and a resolution of 2.0Å.

On 2007 June 19 the telescope was equipped with the Inamori-Magellan Areal Camera and Spectrograph (IMACS: Bigelow & Dressler 2003) to acquire time-resolved spectroscopy of GW Lib. IMACS was used with the f/4 camera

and the long-slit-mask with a 0.7 arcsec slit width and a 600 lines mm^{-1} grating centred at 5550Å. The spectra were dispersed along the short-axis of four SITe CCDs in the IMACS mosaic detector. The CCD detectors were binned two by two during the observations. This instrumental setup provided a dispersion of 0.76Å pixel^{-1} and a spectral resolution of 1.29Å FWHM in the spectral interval $3950 - 7100$Å.

2.1.2   Tillinghast Telescope

The 1.5-m reflector Tillinghast Telescope (TT) equipped with the FAST instrument (Fabricant et al. 1998) acquired 7 epochs of time-resolved spectroscopy and 16 epochs of single spectroscopic frames in service mode. For the time-resolved observations, the FAST instrument was equipped with a 2688 $\times$ 512 UA STA520A CCD chip with a 15 microns pixel size. A grating of 1200 lines mm^{-1} covering $4150 - 5200$Å and a 1.5 arcsec slit width was used to deliver a dispersion of 0.38Å pixel^{-1} and spectral resolution of 0.86Å FWHM.

For the single frames the telescope was used in service mode with a grating of 300 lines mm^{-1} and an aperture of 3.0 arcsec to cover the spectral interval $3300 - 7600$Å. The pixels were binned two by two to give a dispersion of 1.47Å pixel^{-1} and a resolution of 5.9Å.

2.1.3   William Herschel Telescope

On two successive nights, three months after the 2007 outburst, we acquired time-resolved spectroscopic data using the 4.2-m William Herschel Telescope (WHT) in combination with the two-armed Intermediate dispersion Spectrograph and Imaging System (ISIS). The blue arm of the spectrograph was equipped with a 4096×2048 EEV12 CCD. The slit width used was 1.0 arcsec and used with the R1200B grating with 1200 lines mm^{-1} providing a wavelength coverage of $4200 - 5000$Å. This setup delivers a dispersion of 0.224Å pixel^{-1}. The red arm was equipped with a 4096×2048 Red+ CCD with 15 microns pixels. Using the R1200R grating with 1200 lines mm^{-1} the unvingetted wavelength coverage was $8050 - 8800$Å with a dispersion of 0.243Å pixel^{-1}. The spectral resolution for both arms was 0.62Å.

2.2   Reduction

The different sets of spectroscopic data were reduced using several reduction packages.

2.2.1   FAST service mode

The single frame spectra obtained with the FAST spectrograph in service mode were extracted using the spectral extraction pipeline provided by the Telescope Data Center at the Harvard-Smithsonian Center for Astrophysics. This tailored pipeline is based on the IRAF PROCD package, see Tokarz & Roll (1997).

2.2.2   Magellan IMACS

The IMACS data were bias and flat-field corrected in the standard way using IRAF. The spectra were extracted from each

Table 1. Observations of GW Lib

Telescope	Instrument	Date	HJD (start)	Exp time (s)	n spectra	Orbital coverage ($T_{\mathrm{obs}}/P_{\mathrm{orb}}$)	λ - range (Å)	Seeing ($''$)
Magellan	B&C	06/07/2004	2453193.491	60	62	1.00	3500 - 5100	0.5-1.0[a]
		07/07/2004	2453194.471	60	66	1.02		0.7-1.2
TT	FAST	14/04/2007	2454204.859	60	1	–	3300 - 7600	1-2
		14/04/2007	2454204.861	30	2	–		1-2
		20/04/2007	2454210.859	15	2	–		–
		09/05/2007	2454229.833	120	1	–		2
		09/05/2007	2454229.836	300	1	–		2
		11/05/2007	2454231.817	120	2	–		2
		15/05/2007	2454235.813	480	1	–		–
		18/05/2007	2454238.894	600	1	–		–
		20/05/2007	2454240.811	480	1	–		–
		23/05/2007	2454243.787	720	1	–		–
		09/06/2007	2454260.739	720	1	–		–
		16/06/2007	2454267.774	1200	1	–		–
		24/06/2007	2454275.691	1200	1	–		–
TT	FAST	14/04/2007	2454204.886	200	34	1.86	4150 - 5200	1-2
		15/04/2007	2454205.861	60	110	1.75		1-2
		20/04/2007	2454210.882	60	70	1.46		1-2
		23/04/2007	2454213.858	120	37	1.68		1-2
		10/05/2007	2454230.833	300	18	1.75		2
		12/05/2007	2454232.833	600	2	0.16		2
		17/05/2007	2454237.784	300	22	1.94		1-2
Magellan	IMACS	18/06/2007	2454270.531	30	73	1.09	3950 - 7100	0.6
WHT	ISIS	24/07/2007	2454306.365	240	19	1.08	4200 - 5000/8050 - 8800	1
		25/07/2007	2454307.350	240	25	1.35		1-2

[a] From Magellan Guide Camera Seeing at `www.lco.cl`

CCD frame with the IRAF KPNOSLIT package. The pixel-to-wavelength calibration was derived from cubic spline fits to HeNeAr arcs acquired during the observations. Fitting 10 - 20 lines per frame gave a RMS < 0.017Å per chip.

2.2.3   All others

All other data sets were reduced in the following way. The average bias and flat-field correction was carried out using the FIGARO package from STARLINK and nightly average bias and tungsten frames. PAMELA was used for the optimal extraction of the spectra (Marsh 1989). Regular CuAr arc lamp exposures allowed us to establish an accurate wavelength scale for each spectrum through interpolation between the nearest arcs in time. Each arc frame has been fitted with a 5th order polynomial to 10-40 lines to give a typical RMS of 0.1 pixel. The individual spectra were normalised to the continuum level using a spline fit to selected continuum regions.

3   GW LIB IN OUTBURST

The April 2007 outburst of GW Lib triggered our target of opportunity program at the TT. Both time-resolved spec-

troscopy and single frame observations of GW Lib were obtained during this period of activity. See Table 1 for specific details.

3.1   Spectral evolution

In Figure 2 average representative normalised spectra during different stages of the outburst of GW Lib are presented. The bottom spectrum is during quiescence 3 years before the 2007 outburst, the second spectrum is a day after outburst peak, the third during slow decline, the fourth during rapid decline and the fifth during the final decline towards quiescence. For reference, the top frame in Figure 1 shows the outburst light curve in the V-band, as provided by AAVSO and its network of observers. The dates corresponding to the spectra plotted in Figure 2 are marked. The pre-outburst quiescent spectrum is given an arbitrary negative HJD for plotting purposes.

The single frame spectra at different nights throughout the outburst make it possible to trace the evolution of various spectral features. We have measured the equivalent widths (EW) of the lines as a function of the outburst. For the Balmer lines, the overall continuum is normalised but any underlying absorption within the line was not removed. This
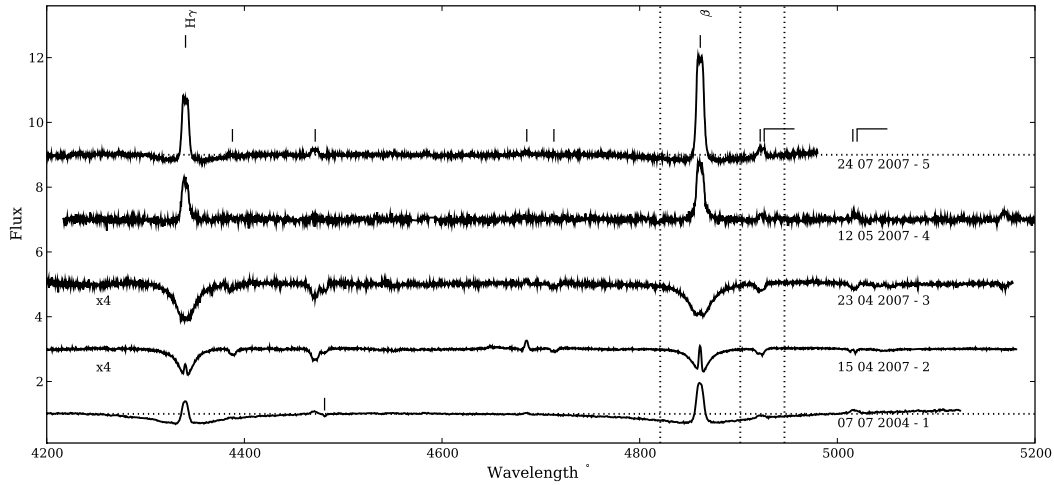
Figure 2. Comparison of average representative normalised spectra of GW Lib sampling the spectral evolution before and during the 2007 super-outburst. The April 2007 spectra have been multiplied by a factor of 4 to magnify the spectral features and allow for a better comparison. The vertical *dotted* lines annotate the ± 2500 km s^{-1} window for the Balmer lines and the ± 1500 km s^{-1} band for helium lines while the horizontal *dotted* lines the normalised continuum flux.
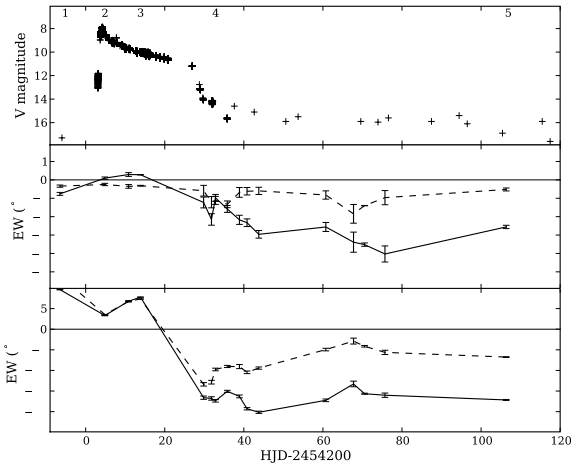

Figure 1. Time evolution of the equivalent widths of the principal spectral lines. The July 2004 quiescent epoch is plotted at an arbitrary negative HJD for comparison. In the bottom frame: *solid* line for Hβ and *dashed* line for Hγ. In the middle panel: *solid* line for He I 4921Å, represents the general evolution of the He I lines and *dashed* line for He II 4685Å. The top panel shows the V magnitude of the outburst, as provided by the AASVO where the numbers indicate position of the spectra from Figure 2 which are discussed epochs in Section 3.1.

results in positive (EW) values during absorption-dominated epochs and negative values otherwise. For consistency, the window for these lines is ± 2500 km s^{-1} for all epochs, which is limited by the proximity of the helium lines. For the He lines, a slightly narrower window of ± 1500 km s^{-1} gives a consistent and comparable EW measurement, avoiding neighbouring lines. The spectra are locally normalised to avoid any contamination from underlying absorption due to nearby Balmer lines. Both regions are marked in Figure 2 together with the continuum level. The bottom panel in

Figure 1 shows the EW evolution for the Balmer lines and the middle panel the same for the helium lines. The actual values for all lines and at all observed epochs are given in Table 2. We note that the spectral lines display rather complex changes as different components come and go. A single (EW) value clearly does not fully capture these details. Therefore, to complement the measured (EW), a more detailed analysis of the separate components within the line profiles is provided below.

2004 July 7 - 1 During deep quiescence, 3 years before outburst, the average spectrum of GW Lib was typical for a CV spectrum with a low accretion rate. The accretion disc has very narrow Balmer emission lines which show a dip in their centres reflecting an underlying double-peaked profile (not visible on the scale of Figure 2). This profile shape is expected for optically thin accretion discs viewed at a low inclination angle i. The Hβ profile is fitted with two Gaussians simultaneously to the absorption trough and the narrow emission line component. The latter gives a FWHM of 7.82 ± 0.56Å corresponding to ~ 482 km s^{-1} (all errors quoted in this paper are 3σ errors). Absorption troughs flank the emission features with a FWZI of $\sim 20,000$ km s^{-1}, and can only originate from the WD as these velocities are too high for Kepler velocities in the accretion disc. This indicates a small accretion luminosity and a very low mass transfer rate such that the primary WD is visible. The measured EW of the Balmer lines are dominated by the WD absorption. The He I lines are all in emission. A small, but significant, amount of He II is present in emission with an EW of -0.34 ± 0.18Å in the average spectrum. Since the disc and companion star are expected to be too cool during quiescence to produce much He II emission, this line emission may be due to the relatively hot WD ionising gas near it. The feature is unfortunately too weak to permit any time-resolved analysis. We also note that an absorption line at Mg II 4481.15Å is present with an EW of 0.24 ± 0.09Å mea-

sured in a ± 300 km s^{-1} window and a FWHM of 3.18 ± 0.35Å. This is likely formed in the photosphere of the WD and such metal lines may be expected in accreting systems were metal-rich gas is deposited onto the WD surface. The determination of the gravitational redshift of such lines could in principle provide a direct measurement of the mass of the WD. However, our resolution prohibits a reliable measurement of the velocity of this weak feature as it is blended with the nearby He I line.

2007 April 15 - 2 Two days after the rise into outburst started, the average spectrum of GW Lib shows broad absorption troughs in the Balmer lines. Given the 9 magnitude increase due to accretion these absorption features can no longer be associated with the WD but suggest an origin in the now optically thick accretion disc, supported by a FWHM of 23.05 ± 0.36Å. The lines also show strong emission peaks, see spectrum 2 in Figure 2. This is also seen in the Hα emission profile obtained by Hiroi et al. (2009) around this time. With a FWHM of only 3.14 ± 0.66Å, corresponding to ~ 194 km s^{-1}, the peak in Hβ has less than half the width of the emission during quiescence. The He I lines are all in absorption, with a hint of a very narrow emission peak at the centre, while the He II line at 4685Å is in emission at EW $= -0.25 \pm 0.19$Å. Finally Fe is marginally detected in absorption. We will revisit the discussion on the origin of these lines in section 3.2.

2007 April 23 - 3 Ten days after the beginning of the outburst, GW Lib slowly started to fade and the spectrum evolved. The strong and narrow emission in the Hβ and Hγ lines decreased in strength, increasing the overall EW slightly. The EW of the He I lines increases similarly suggesting the same narrow emission was indeed present. The accretion disc is still visible as an optically thick disc in absorption in the Balmer lines with a FWHM of 30.46 ± 0.26Å. The He II emission decreases slightly to an EW of -0.32 ± 0.06Å.

2007 May 12 - 4 A month after outburst, as the system dropped from the outburst plateau (Figure 1) and the luminosity decreased rapidly, the spectrum had changed drastically, see spectrum 4 in Figure 2. The accretion disc contribution to the lines changed from an optically thick flow back into a chiefly optically thin disc, producing shallow double-peaked emission profiles in the Balmer line without the high velocity absorption, leading to a negative EW. The emission component in Hβ is visible again and now has a FWHM of 8.59 ± 0.03Å, close to the value of the pre-outburst emission line. As can be seen in Figure 1, the EWs of all lines make a small jump. WZ Sge type DNe often show brief brightenings shortly after their main outburst, referred to as echo-outbursts (Patterson et al. 2002). It remains unclear due to the sparse light curve sampling whether the observed behaviour in the lines is related to similar events.

2007 June 19 The Magellan spectra from June 2007 resemble the WHT July spectra in shape, see top spectrum in Figure 2 for the average spectrum. In addition, these spectra also cover the Hα and the He I 5876.62Å line. An interesting feature next to the strong He I line is the Sodium doublet (Na D 5889.95Å-5895.92Å) seen in emission, see Figure 3.

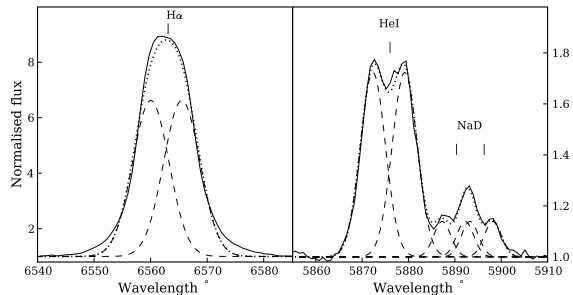**Figure 3.** Normalised emission line profiles of Hα (left) and the He I - Sodium doublet (right). The *solid* line represents in both cases the average profile over 1 orbital period. The *dashed* lines are the various Gaussian profiles fits and the *dotted* line is the sum of all single Gaussians. As is clear from these fits, the Sodium doublet has, most likely, a very similar origin as the Hα and the He I lines.

Due to the close proximity of GW Lib, interstellar absorption is expected to be weak, and indeed no evidence for diffuse interstellar band (DIB) absorption features can be found in the spectrum. Instead, the doublet is dominated by broad emission components. To strengthen this case, the Sodium doublet is also present in emission at 6154.23Å-6160.76Å. In the orbital average spectrum, the feature can be fitted with two double Gaussians (plotted in Figure 3) with the peak separation set to 250 km s^{-1}. The Hα line has the same separation where for the nearby He I the line separation is 350 km s^{-1}. The offset of the centre of the double-peaked profiles from the rest wavelength for all lines is, within errors, -10 ± 5 km s^{-1}. These similar fitting values suggest a shared origin in the accretion flow for all lines. Time-resolved analyses of the He I and the Balmer lines give similar values compared to those in the July 2007 epoch (see section 4.2 and Table 4).

2007 July 24 - 5 Three months after outburst, during the slow decline towards quiescence, the system was still 1-2 mags brighter than the pre-outburst magnitude, and the double-peaked profile from the disc proved stronger against the dropping continuum compared to the previous phase (compare spectrum 4 to spectrum 5 in Figure 2). The system has cooled sufficiently such that the WD absorption again flanks the emission lines in the Balmer lines, decreasing the EW of Hγ. Since both the disc and the WD are expected to be slightly hotter and brighter compared to the pre-outburst quiescence state it does not yet resemble spectrum 1 in Figure 2. For comparison, the WD in WZ Sge was still cooling after 17 months of post-outburst observations, see Long et al. (2004). The He I lines are all in emission and the He II emission line has an EW of -0.52 ± 0.24Å. The FWHM of the emission component in Hβ is 7.65 ± 0.03Å and has thus reached the value observed in the pre-outburst epoch even though the emission line flux itself is still much larger.

3.2 Time-resolved spectra

Several epochs (see Table 1) of time-resolved spectroscopy allows us to characterise the line behaviour in more detail. During outburst, these time-resolved spectra showed

Table 2. Equivalent widths in Å $\pm3\sigma$ error, of various emission lines as function of the outburst. The Balmer lines are measured in a ±2500 km s^{-1} window, where the helium lines are measured in a ±1500 km s^{-1} window

Epoch	HJD (start)	Hβ	Hγ	HeI 4387	HeI 4471	HeII 4685	HeI 4921
1	2453194.471	9.61 ± 0.18	12.93 ± 0.15	-0.29 ± 0.18	-0.74 ± 0.12	-0.34 ± 0.18	-0.76 ± 0.24
2	2454204.859	3.32 ± 0.16	3.55 ± 0.17	0.04 ± 0.18	0.47 ± 0.18	-0.25 ± 0.19	0.10 ± 0.19
	2454210.859	6.79 ± 0.37	6.75 ± 0.37	0.04 ± 0.30	1.19 ± 0.30	-0.35 ± 0.30	0.29 ± 0.31
3	2454213.858	7.78 ± 0.07	7.32 ± 0.09	0.50 ± 0.06	1.03 ± 0.07	-0.32 ± 0.06	0.28 ± 0.03
	2454229.833	-16.61 ± 1.19	-13.37 ± 1.26	0.29 ± 0.91	-2.84 ± 0.97	-0.59 ± 0.87	-1.23 ± 0.89
	2454231.817	-16.80 ± 1.23	-12.85 ± 1.33	-0.00 ± 0.98	-1.30 ± 0.98	-1.21 ± 0.92	-2.15 ± 0.94
4	2454232.833	-17.37 ± 0.90	-9.77 ± 0.95	-0.96 ± 0.62	-0.01 ± 0.62	-1.11 ± 0.65	-0.98 ± 0.56
	2454235.813	-15.07 ± 0.74	-9.04 ± 0.78	-0.36 ± 0.58	-0.84 ± 0.57	-1.33 ± 0.55	-1.58 ± 0.56
	2454238.894	-16.30 ± 1.01	-9.06 ± 1.48	-0.83 ± 1.07	-1.06 ± 0.95	-0.68 ± 0.80	-2.17 ± 0.74
	2454240.811	-19.30 ± 0.84	-10.46 ± 0.94	-1.15 ± 0.71	-1.43 ± 0.66	-0.62 ± 0.61	-2.33 ± 0.62
	2454243.787	-20.15 ± 0.82	-9.43 ± 0.82	-1.51 ± 0.64	-1.32 ± 0.62	-0.60 ± 0.59	-2.96 ± 0.62
	2454260.739	-17.25 ± 0.95	-4.94 ± 0.93	-1.09 ± 0.74	-0.29 ± 0.68	-0.82 ± 0.68	-2.56 ± 0.73
	2454267.743	-13.28 ± 2.05	-2.88 ± 2.15	-0.57 ± 1.67	-0.74 ± 1.54	-1.84 ± 1.53	-3.39 ± 1.64
	2454270.531	-15.65 ± 0.41	-4.14 ± 0.57	-0.65 ± 0.46	-2.04 ± 0.42	-1.40 ± 0.30	-3.52 ± 0.27
	2454275.691	-16.01 ± 1.58	-5.62 ± 1.54	-1.32 ± 1.28	-3.62 ± 1.26	-0.97 ± 1.16	-4.03 ± 1.31
5	2454306.355	-17.16 ± 0.35	-6.76 ± 0.27	-0.75 ± 0.24	-1.47 ± 0.21	-0.52 ± 0.24	-2.56 ± 0.27

considerable orbital dependence in the Balmer, He I and He II line profiles. We binned the spectra in bins of 1/20th of the orbital period using $P = 0.05332 \pm 0.00002$ days (Thorstensen et al. 2002). The Balmer profiles were fitted with a double Gaussian with the peak, FWHM and the offset from the rest wavelength as free parameters. The He I and He II profiles are fitted with a single Gaussian. All fits show that the peak and FWHM of the line components are constant within 10 per cent of their average values and as these particular parameters show no sign of significant orbital dependence, they were thus fixed to their mean values for further analysis, keeping their velocity offsets as free parameters. In addition to our profile fits, all results were checked against a traditional double Gaussian analysis (Schneider & Young 1980) in combination with a diagnostic diagram.

The radial velocity curves of our line components were fitted with the function $V(\phi) = \gamma - K\sin(2\pi\phi - 2\pi\phi_0)$ and individual velocity data points were weighted according to their errors as derived from the profile fits. These errors were scaled such that the radial velocity curve fit has a goodness of fit close to 1. Here γ is the systemic velocity, K the radial velocity semi-amplitude of the absorption and/or emission line and ϕ_0 the phase offset relative to the ephemeris. The ephemeris zero point will be derived later in this paper (section 4) and is used throughout this paper when calculating orbital phases. Due to the lack of precision in the binary orbital period, the ephemeris cannot be extrapolated very far in time and thus the binary phase is arbitrary except for the July 2007 epoch where the zero-point is measured.

We discuss the results of the fits for the Hβ and He II profiles using the 2007 April 15 data as this set has the highest signal to noise, the best time resolution and the most features present for analysis. The behaviour of the lines during the other nearby epochs were the same, albeit determined with lower precision. The results can be found in Figure 4 and Table 3. Both Hβ and Hγ have similar amplitude and phase fits. The deep and broad absorption troughs can be identified with the accretion disc. However, they do not trace the WD movement as the velocity semi-amplitude is too

large at 51.3 ± 6.5 km s^{-1}. The radial velocity of the primary WD is likely much smaller. Interestingly, this amplitude is consistent with that of the double-peaked emission profile during quiescence. On 2004 July 6, the velocity curve fit to Hβ emission gives a semi-amplitude of 45.1 ± 7.3 km s^{-1}. This similarity suggests that the distortions in the disc leading to the observed radial velocity curve of both the disc emission during quiescence and the broad disc absorption during outburst are rather similar. Unfortunately, due to the uncertainty in the binary ephemeris, we cannot compare their relative phasing. Similar amplitudes, systemic velocities and phase zeros were found for the He I lines, suggesting that their profiles trace the same components. In contrast, the He II line moves in anti-phase and has half the amplitude. This highlights the difficulty with associating either of these radial velocity amplitudes with that of the primary WD.

In both the Hβ and Hγ profile, a second Gaussian is fitted to the narrow emission components in their cores. This component shows a remarkably small velocity amplitude of 3.0 ± 1.6 km s^{-1} (see Table 3). At this epoch, the arc fit is good to 0.003Å at the position of Hβ which is smaller than 1/100th of the 0.38Å/pixel scale. 1σ errors on individual velocity measurements are much larger ($\sim$0.085 pixels) than this and are thus dominated by the statistical error. These errors are then propagated to provide the formal errors on the fit parameters as listed thus suggesting that this small amplitude is measured to a significant degree.

This strong central emission component is present in those epochs close to the start of the outburst in the Balmer lines and a hint is present in the He I lines. On 2007 April 20 the dynamics of this component is similar to behaviour on April 15. By 2007 April 23 the emission component has faded into the absorption lines, which maintain their radial velocity semi-amplitude throughout. The systemic velocity of this narrow emission component is consistent with that of the He II emission, while the broad absorption components in the Balmer lines have a rather different γ which is perhaps due to a slowly precessing disc.

Table 3. Velocity profile parameters on 2007 April 15

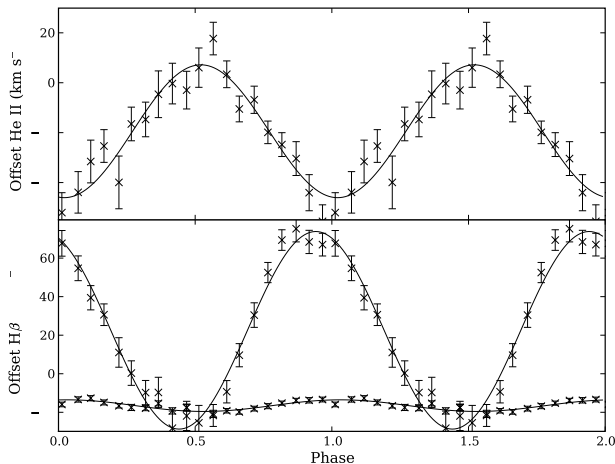| Line	γ $\mathrm{km\,s^{-1}} \pm 3\sigma$	K $\mathrm{km\,s^{-1}} \pm 3\sigma$	ϕ_0 $\pm 3\sigma$	Identification
Hβ emission	-16.6 ± 0.8	3.0 ± 1.6	0.28 ± 0.06	Slingshot/WD?
Hβ absorption	22.5 ± 4.4	51.3 ± 6.5	0.19 ± 0.02	Accretion disc
Hγ emission	$-$	$-$	$-$	$-$
Hγ absorption	17.0 ± 4.8	43.6 ± 6.8	0.18 ± 0.02	Accretion disc
He II emission	-19.4 ± 4.7	26.6 ± 6.8	0.77 ± 0.04	$-$

Figure 4. Top panel shows the radial velocity curve of the He II emission. The radial velocity curves of the Hβ profile (bottom) are fitted with a low amplitude emission component and a high amplitude absorption component. Both are from the phase-binned 2007 April 15 data, showing two orbital cycles.

GW Lib is one of the few CVs that have been followed through the outburst spectroscopically. For comparison, the spectral evolution of SS Cyg (figure 5 in Hessman et al. 1984) showed broad, double-peaked emission lines that are gradually being overtaken by the rising continuum, followed by the formation of line wings in absorption. This qualitative behaviour is expected as the accretion disc makes a rapid change from a low $\dot{M}$ optically thin configuration to a high $\dot{M}$ optically thick flow at the onset of the outburst. Near maximum light, SS Cyg shows on top of the absorption from the accretion disc, narrow emission cores which decay again after outburst. These are very similar to the spectral changes presented here for GW Lib, though no dynamical properties are available to compare the components quantitatively. Unfortunately, the very low binary inclination of GW Lib makes it difficult to study the accretion disc dynamics during the main outburst period. The absorption dominated disc lines are unsuitable for Doppler tomography and we therefore cannot search for disc asymmetries such as the tidal spirals seen in other DNe (e.g. IP Peg: Steegs, Harlaftis & Horne 1997; U Gem: Groot 2001). When disc emission returns, little structure can be detected in its marginally double-peaked lines.

The stationary emission component in the spectra, visible only during the first couple of days of the outburst, does not obviously fit in with the typical components expected to dominate the line emission in a mass transferring binary system. The low velocity suggests a location near the centre of mass in the orbital plane or along the axis through the centre of mass, perpendicular to the orbital plane. GW Lib is not the first DN to show these features. Several DN systems have been reported to show low amplitude strong emission components in the Balmer lines.

Steeghs et al. (1996) report low velocity emission components in the Hα and He II 4686Å lines of the DNe IP Peg and SS Cyg and proposed slingshot prominences from the donor star as a possible origin for these features since their known system parameters rule out an origin near either the WD or the surface of the donor star. The rapidly co-rotating donor star may form prominences and such magnetic loops would be pulled towards the WD and could potentially find an equilibrium in between the L1 point and the WD. As the prominence material is illuminated by the disc during outburst, it becomes visible as an emission source which is co-rotating with the binary orbit but located in the region near the centre of mass and thus displays very little radial velocity. If we follow their recipe, the observed Hβ/He II ratio is consistent with a gas temperature in the 10,000 - 15,000 K range.

In GW Lib, an alternative origin of the low-velocity emission may be near the surface of the WD, if its orbital velocity (K_1) is very small. Low state AM CVn systems often show such narrow emission components (Morales-Rueda et al. 2003, Roelofs et al. 2006). The low mass ratio derived from the late superhump by Kato, Maehara & Monard (2008) together with the low orbital inclination would indeed imply a very low value for K_1 in GW Lib. We will revisit these interpretations and the implications for the system parameters in section 5.

4   GW LIB POST OUTBURST

Binary evolution tells us that the majority of the current CV population should have evolved towards short orbital periods with the mass donor star depleted to a low mass degenerate brown dwarf (e.g. Knigge 2006, Kolb & Ritter 1992, Rappaport, Verbunt & Joss 1983). Not only has this graveyard of CVs been elusive for many years (see Gänsicke et al. 2009), our sample of short period CVs with reliable binary parameters, other than the orbital period, is very small. This is mainly due to the fact that despite the low mass transfer rates, the donor stars are extremely faint and it is very difficult to perform traditional radial velocity studies using photospheric

absorption lines from the donor. Most studies are confined to using the strong Balmer emission lines to try and constrain system parameters (e.g. table 2 in Marsh 2001, Southworth et al. 2007, Neilsen, Steeghs, & Vrtilek 2008, Mennickent, Unda-Sanzana & Tappert 2006, Szkody, Desai & Hoard 2000). The Ca II triplet at 8498.03Å, 8542.09Å and 8662.14Å[1] offers advantages that more than make up for its relative weakness compared to the Balmer lines. It has a lower ionisation energy than either hydrogen and helium and is thus capable of being excited even by cool sources of radiation, and its thermal width and pressure broadening are much smaller than for hydrogen leading to sharper, more easily detected spikes of emission (Marsh & Dhillon 1997). Studies have shown that Ca II is also more accessible than the Balmer lines for the study of velocity gradients and turbulence. This is because the thermal velocity broadening is smaller in general and the Keplerian shear broadening starts to dominate at higher inclinations compared to the hydrogen lines (Horne 1995). These studies show a promising, but so far neglected avenue for emission line studies of CVs. The average normalised spectrum of GW Lib in the I-band obtained on 2007 July 24 is plotted in Figure 5 and shows a strong Ca II triplet in emission.

4.1 Emission from the secondary

In Figure 6 (middle panels), we compare trailed spectrograms of Hβ (left) and Ca II 8662Å (right) as obtained 3 months after outburst. Whereas the Balmer line shows a shallow double-peaked profile and a rather blurry trail, the Ca II trail is much sharper even at a lower S/N. It shows a clear double-peaked profile from the accretion disc and an S-wave moving in between. No such S-wave appears to be present in the Balmer lines.

To highlight this component, we averaged the profiles in a frame co-moving with the S-wave and show these in the top panels of Figure 6. The double-peaked profile from the accretion disc in this frame is averaged out, but the narrow S-wave is clearly visible on top on the broad profile in the Ca II case whereas its absence is noted in the Balmer profile.

The S-wave is sharp and its amplitude is smaller than the velocity offset of the accretion disc peaks, suggesting it may originate from the secondary star rather than from the interaction point between the infalling stream and the accretion disc, the hotspot, since the latter would have a velocity equal to or larger than the outer disc edge.

Assuming the emission does indeed arise from the surface of the donor star, the ephemeris can be determined as the crossing from blue-to-red of its velocity curve, which corresponds to inferior conjunction. This gives:

$$\mathrm{HJD} = 2454307.36867 + 0.05332E$$

This is used throughout the paper to define the orbital phase although the accuracy of the orbital period is not enough to give the outburst data discussed in Section 3 a definite orbital phase since the accumulated uncertainty is too large (Figure 7).

The radial velocity semi-amplitude of the emission is determined using two different methods. The first method is the fitting of a Gaussian to the S-wave line component followed by a radial velocity curve fit. The second method is the localisation of the emission peak in the velocity-velocity plane using Doppler tomography.

For the first method, the spectra are phase-binned and a triple Gaussian profile with as variables the offsets, the peak heights and the FWHMs of the profiles is fitted where two Gaussians trace the disc features and the third is for the donor S-wave. Both the peak height and the FWHM show a chaotic variability with a maximum amplitude of 8 per cent from the average value and were therefore fixed to their mean values, leaving just the velocity offset as fit parameter. The offset velocity for the S-wave emission is plotted in Figure 7 together with a weighted radial velocity curve fit. For improved accuracy in the Ca II triplet, we performed a joint fit to the 3 triplet lines with a common velocity offset. We then find a semi-amplitude of $K_{\mathrm{Ca\ II}} = 82.2 \pm 4.9$ km s^{-1} for the S-wave in the Ca II profiles, see also Table 4.

To complement our radial velocity fits, Doppler maps are created with a Maximum Entropy Method (MEM; Marsh 2001) for both the Balmer and the Ca II 8662Å lines, see bottom panels in Figure 6 for MEM map of the time-resolved spectra on 2007 June 24. Given the fact that the lines from the Paschen series overlap with the Ca II triplet lines, we always ensured that the Doppler reconstructions fitted to both lines simultaneously. The underlying Paschen line distribution is rather featureless, and the sharp S-wave component is only present in the Ca II reconstructions. Even if such a Paschen contribution is not included, the Ca II tomograms show very similar features.

The Balmer map (bottom left panel) shows a diffuse ring of emission from the accretion disc. Due to the sharper line profile, the Ca II map (bottom left panel) shows a much better defined accretion disc ring with a significant asymmetry at phases ~ 0.10, ~ 0.35 and ~ 0.70. Furthermore, the S-wave component manifests itself as a sharp emission spot peaking at a velocity of $\sim 85 \pm 5$ km s^{-1}. Its location relative to the disc ring is as expected for donor emission and thus the CaII S-wave is revealing the secondary in GW Lib for the first time.

4.2 Emission from the accretion disc

With the outburst activity decaying away, the disc contribution to the overall luminosity decreases and significant regions that are optically thin start to re-appear. These give rise to the characteristic double-peaked profile visible in both the Balmer lines and the Ca II lines. A single broad Gaussian profile fit to this feature in the phase-binned spectra together with a weighted radial velocity fit for both the Ca II and Balmer profiles at multiple nights gives an average value for the amplitude of the disc of $K_{\mathrm{acc}} = 19.2 \pm 5.3$ km s^{-1}, see Table 4. Similar results are obtained using multiple Gaussian line fits and diagnostic diagrams with double Gaussians. This amplitude is significantly different from the amplitude of disc related features in the April 2007 and July 2004 data. The phase shift of both Ca II and the Balmer disc coincide but are not in anti-phase with the donor star with respectively $\phi = 0.68 \pm 0.04$ and $\phi = 0.73 \pm 0.04$. They cannot directly track the WD and thus

---

[1] From The Atomic Line List Version 2.04: `http:/www.pa.uky.edu/~peter/atomic/`

Table 4. Velocity profile parameters on 2007 June 25

Line	γ $\mathrm{km\,s^{-1}} \pm 3\sigma$	K $\mathrm{km\,s^{-1}} \pm 3\sigma$	ϕ_0 $\pm 3\sigma$	Identification
Balmer emission	-7.6 ± 5.6	19.2 ± 5.3	0.68 ± 0.04	Accretion disc
Ca II emission	20.6 ± 3.3	19.8 ± 4.2	0.73 ± 0.04	Accretion disc
Ca II emission	-13.1 ± 3.7	82.2 ± 4.9	0.00 ± 0.01	Donor star
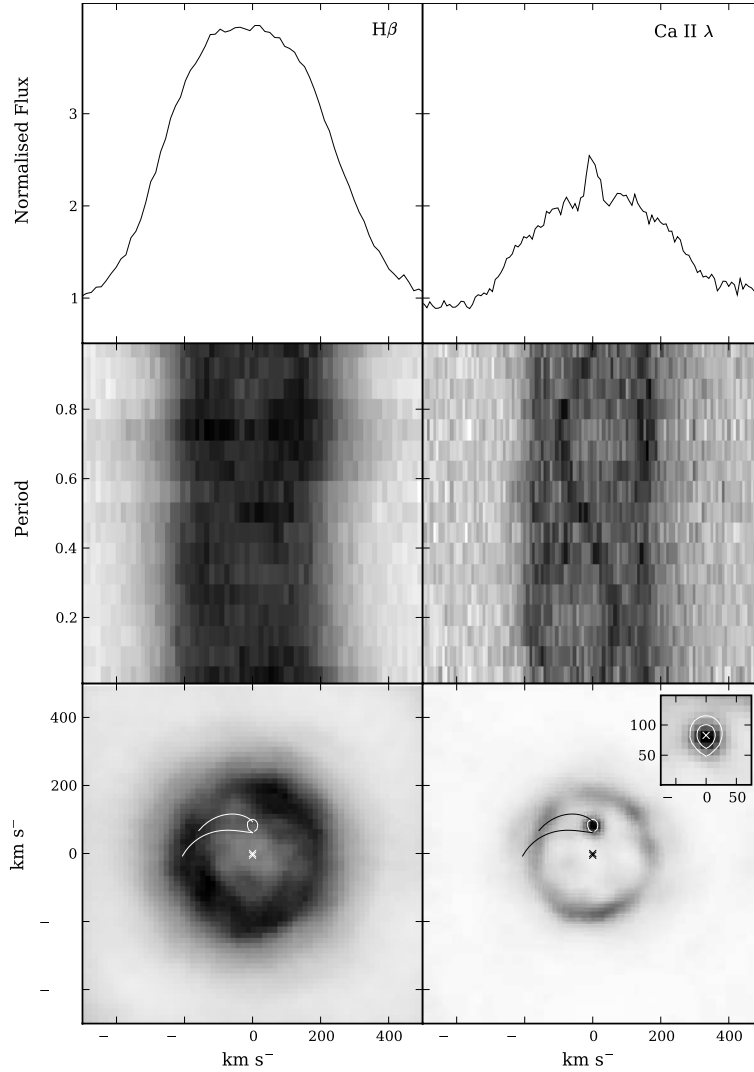
Figure 6. Comparison of the dynamics of the Balmer lines (Hβ, left column) versus Ca II (8662Å, right column). The top row show average profiles in the reference frame of the donor star S-wave. The sharp donor component stands out in Ca II but the Hβ profile is smooth. The middle row shows the phase-binned trailed spectrograms. The S-wave can be traced in between the disc peaks in Ca II only. The bottom row plots the Doppler tomograms showing the superior sensitivity and sharpness in the Ca II lines. The S-wave is mapped to a sharp spot consistent with donor star emission. Overlaying the Doppler tomograms are the positions of the WD, the Roche Lobe of the donor star and the streams for a model with $q = 0.062$. The inset in the Ca II Doppler map shows the Roche Lobe on the Donor star in more detail for both a $q = 0.062$ and $q = 0.23$ solutions.
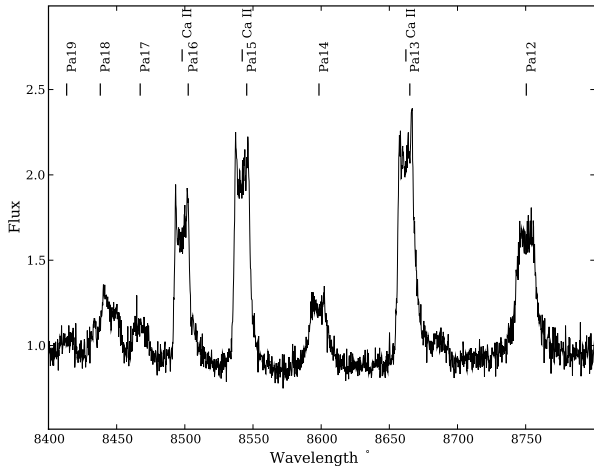
Figure 5. The average normalised I-band spectrum of GW Lib on July 24, 2007 showing the Paschen series and the double-peaked Ca II lines.
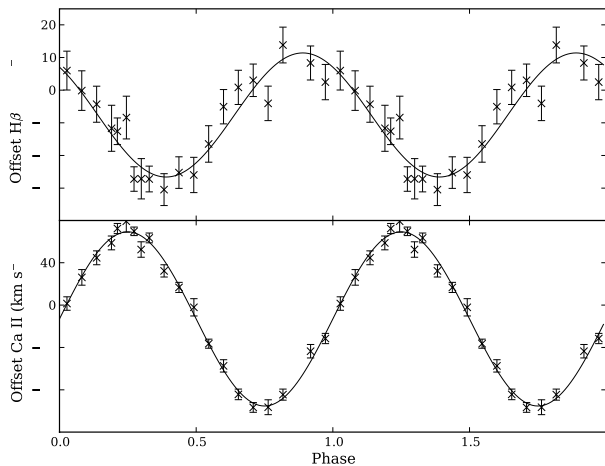

Figure 7. Top panel shows the radial velocity curve of the Hβ emission. The bottom panel shows rotational velocity curve from the Ca II 8662Å S-wave emission component. Both are from the phase-binned 2007 June 24 data, showing two orbital cycles.

the radial velocity amplitude is disturbed by some residual disc asymmetry and cannot be straightforwardly connected to K_1.

The accretion disc in the Doppler maps of Hβ appears rather featureless with little azimuthal structure, while the Ca II trail and MEM map show lower intensity in the disc around phases ~ 0.10, ~ 0.35 and ~ 0.70. The centre of emission of the discs for both maps was determined by looking at their centre of symmetry. To determine the optimal centre of symmetry of the disc, we subtracted a symmetrical component from both the Ca II and the Hβ Doppler map centred at V_x, V_y in the ranges of -100 – +50 km s^{-1} making grid steps of 2 km s^{-1} and inspected the residuals in the lower half of the map (see also Steeghs & Casares 2002). The best fits are found for $V_x = 0.0 \pm 5.0$ km s^{-1} and

$V_y = -6.0 \pm 5.0$ km s^{-1} for the Ca II map. The fits for the Hβ give identical values but with a larger error. The low V_x is encouraging from the point of view of linking the disc centre with the WD at $(0, -K_1)$. The implied $K_{\text{disc}} = -V_y = 6$ km s^{-1} is smaller than the semi-amplitude derived using the Gaussian fits. On the other hand they are formally consistent when considering our error estimates, and both point to a small K_1.

4.3 Systemic velocity

The binary systemic velocity (γ) is a quantity that should obviously be the same in all spectral lines, reflecting the fixed radial velocity of the binary system with respect to us. For different lines at different epochs, the systemic velocity was determined using two methods.

The first method determines the systemic velocity as derived from the radial velocity curve discussed previously, see Tables 3 and 4. For the Balmer lines associated with the accretion disc $\gamma = -26 \pm 6.7$ km s^{-1} before outburst, during outburst $\gamma = 22.5 \pm 4.4$ km s^{-1} and after outburst $\gamma = -7.3 \pm 3.6$ km s^{-1}. The narrow Hβ emission during outburst has $\gamma = -16.6 \pm 0.8$ km s^{-1}. For our Ca II profiles, we found $\gamma = 20.6 \pm 3.3$ km s^{-1} for the disc emission and $\gamma = -13.1 \pm 3.7$ km s^{-1} for the donor star emission line. The latter is the most reliable value for γ as the donor star has to move with the systemic velocity.

The alternative method uses the dependence of MEM maps on the assumed systemic velocity. Reconstructed emission spots in the map have optimal sharpness at the correct value for γ, while reconstructions at significantly different values will broaden the features and introduce possible artefacts. Ranging γ between -50 – +20 km s^{-1} in steps of 5 km s^{-1} gives the best reconstruction for $\gamma = -15 \pm 5$ km s^{-1}.

Our various estimates therefore point towards a γ of -15 ± 5 km s^{-1}, in agreement with the measurements by Szkody, Desai & Hoard (2000). The only outliers are the Balmer absorption line during outburst with a systemic velocity fit of 22.5 ± 4.4 km s^{-1} and the Ca II emission associated with the accretion disc with $\gamma = 20.6 \pm 3.3$ km s^{-1}. However, those fits are distorted as the resolution is not sufficient to properly resolve the donor star S-wave and the disc emission peaks near phases 0.25 and 0.75. Subtraction of the S-wave changes and fitting the disc emission with a two-Gaussian profile with an fixed offset between the Gaussians gives a lower value of $\gamma = 7 \pm 2$ km s^{-1}.

5 SYSTEM PARAMETERS

In the previous section we have seen the superior sensitivity of the Ca II emission lines over the commonly observed Balmer lines. Not only do they provide a much sharper view on the accretion disc emission, the key result was the presence of an emission spot from the donor star. This has provided the first ever proxy for its orbital velocity.

Post-outburst radial velocity curves together with Doppler maps have given us estimates of the semi-amplitudes for the different components in the binary system. From both the Balmer and Ca II double-peaks, the radial velocity of the accretion disc was found to be $K_{\text{acc}} = 19.2 \pm 5.3$ km s^{-1}. However, this value may be biased by

disc asymmetries and the donor star S-wave. The observed phase-shift between the disc peaks and the donor does indeed suggest such a bias to be present, while the centre of symmetry searches returned lower K_1 estimates. We therefore consider $K_{\rm acc}$ from the disc peaks as an upper limit on the radial velocity of the WD: $K_1 < K_{\rm acc}$.

The donor star is detected in the Ca II emission as a third peak on top of the accretion disc emission and gives $K_{\rm em} = 82.2 \pm 4.9$ km s^{-1}. Considering the faintness of the low mass donor star, this is unlikely to be powered by chromospheric emission. In any case, the Ca II triplet in chromospherically active stars is generally seen in absorption (e.g. Kafka & Honeycutt 2006) and thus cannot explain the emission seen in GW Lib. A more likely origin is photo-ionisation in the irradiated hemisphere of the donor star facing the WD. The measured radial velocity semi-amplitude is then an underestimate of the true orbital velocity of the donor star ($K_2 > K_{\rm em}$) since not all of the Roche lobe contributes. We calculated the magnitude of this bias, referred to as the K-correction, by simulating the expected emission profiles from an irradiated Roche lobe filling star. Synthetic profiles were calculated for relevant binary parameters including possible shielding of the equatorial regions of the donor by a vertically extended accretion disc.

The peak intensity of the donor star S-wave does not vary significantly as a function of the orbital phase, and instead scatters around a mean value with an RMS of 8 per cent, which is consistent with photon noise. The model profiles discussed above were also used to generate expected orbital light curves of the donor star emission as a function of binary parameters. Model light curves, assuming that the emission is optically thick and thus should be weighted with the projected area, produce orbital modulations above what is observed. However, if we consider more isotropic emission, the modulation disappears at low orbital inclinations. This optically thin model is more appropriate for emission stimulated by photo-ionisation and thus the observed lack of variability is consistent with an irradiated secondary observed at low inclinations.

We can now derive conservative limits on the radial velocities of the stellar components in the system using various methods and spectral lines. They can be summarised as $K_2 > 82.2 \pm 4.9$ km s^{-1} and $K_1 < 19.2 \pm 5.3$ km s^{-1}. These limits translate into a hard upper limit for the mass ratio of $q < 0.23$ regardless of the magnitude of the K-correction or the K_1 overestimate.

After the April 2007 outburst, two detections of superhumps have been reported. Copperwheat et al. (2009) detect a periodicity with a period excess of 4.12 min which implies a mass ratio of $q \simeq 0.211$ if interpreted as a superhump and the empirical superhump-excess mass ratio relation from Patterson et al. (2005) is applied. This is close to our hard upper limit for the mass ratio. However, the authors themselves question the character of the humps and the implied donor stars mass in combination with the WD mass from seismology. On the other hand, Kato, Maehara & Monard (2008) report a superhump period of 0.053925(4) days and a late superhump period of 0.054156(1) days which imply an extreme mass-ratio of $q = 0.062$.

We looked at a simple model for the relation between M_2, K_1 and K_2 as function of q for a range of M_1. Combining this with the above upper and lower limits for the radial

Table 5. Derived system parameters for GW Lib using M_1 from Townsley et al. (2004). The left hand column lists the binary parameters derived from the formal solution based on the measured limits for K_1 and K_2. The right hand column lists the parameters when combining the mass ratio inferred from superhumps with the calculated K_2 from the Ca II $K_{\rm em}$.

	$q \lesssim 0.23$	$q = 0.062$
M_1 ($M_\odot$)	1.02	1.02
K_2 (km s^{-1})	> 82.2	100.8 ± 7.1
K_1 (km s^{-1})	< 19.2	6.2 ± 0.4
M_2 ($M_\odot$)	< 0.23	0.063
v_1 (km s^{-1})	< 122	34
v_2 (km s^{-1})	> 488	548
i ($^\circ$)	> 9.4	10.6 ± 0.8
SpT	M3.9-M5	M8-T

velocities of respectively the WD and donor star rules out systems with $M_1 < 0.75 M_\odot$. As the system is tidally locked, the rotation period of the secondary is equal to the rotation period of the system. Emission lines are broadened by the rotation of the secondary star where the surface velocity can be approximated by looking at the co-rotating Roche Lobe surface. Comparing the measured FWHM of the emission line to the theoretical value as a function of the mass ratio can provide another limit on q and M_1. The observed FWHM of Ca II line emission peak in each bin ranges between 1.0 and 2.2Å due to contamination with the double-peaked profile. The FWHM is very close to the resolution of the data, 0.617Å, which equates to a $v \sin i$ of 21 km s^{-1}. The profile is thus at best marginally resolved. From the upper limits for the mass ratio and the constraints given by the measured emission line broadening we get a rough estimate of the WD mass at $1.0 M_\odot \pm 0.25$, in agreement with the mass determination by Townsley et al. (2004). Note that their window of solutions is constrained by the UV-flux of the WD in combination with the measured distance to GW Lib. For a parallax distance of 104^{+30}_{-20}pc (from Thorstensen 2003) they calculate $M_1 = 1.03 - 1.36 M_\odot$, superseding the previous estimates by Szkody et al. (2002) and Thorstensen et al. (2002) that were based on a larger distance. For further analysis we will use the asteroseismologicaly suggested mass for M_1.

When considering the empirical CV donor sequence of Knigge (2006) at the orbital period of GW Lib, we find a typical pre/post period bounce secondary star mass of $M_2 = 0.064 \pm 0.001 M_\odot$ or $M_2 = 0.060 \pm 0.001 M_\odot$, respectively. The small difference is due to the orbital period being very close to the bounce period. Knigge also calculates the expected absolute magnitudes for GW Lib in the infrared bands using its parallax distance, which implies a low mass secondary star of $0.080 \pm 0.005 M_\odot$.

5.1 Formal solution: $q \lesssim 0.23$

The formal scenario assumes that corrections that need to be applied to our K_1 and K_2 constraints are modest. Thus implying that the mass ratio is near its limit: $q = K_1/K_2 \lesssim 0.23$. The right hand column in Table 5 list the derived system parameters for this ratio. Thorstensen et al. (2002) calculated the inclination based on the FWHM of the shallow peaked Balmer emission lines in quiescence compared to the

FWHM of WZ Sge and found $i \sim 11°$. This is in agreement with our calculations in combination with the nominal solution for $M_1 = 1.02\,M_\odot$ and confirms that GW Lib is indeed observed at very low inclination.

For $q < 0.23$, the correction for K_2, as derived from our models, is at most $\Delta K_{\max} = 35$ km s^{-1} giving a maximum value for K_2 of 118 ± 5 km s^{-1}.

The main problem with a high value for q near our limit is that the secondary would then need to be a $M_2 \sim 0.23\,M_\odot$ mass star with a spectral type around M4-M5 (Cox 2000). In that case, spectral features should be visible in a high resolution, high signal to noise red spectrum. We cannot identify any of such in our post-outburst I-band spectra nor in the pre-outburst Magellan data. Additional issues are the observed IR magnitudes of GW Lib which imply a faint donor and a main-sequence object near $0.23\,M_\odot$ would not fit within the Roche-lobe. All adding to the conclusion that the mass-ratio in GW Lib is likely not near this maximum value.

5.2 Superhump solution: $q = 0.062$

Measuring the late superhumps in GW Lib, Kato, Maehara & Monard (2008) found an extreme mass ratio for the system of $q = 0.062$. Which, when combined with the WD mass from seismology and the empirical donor star mass from the Knigge (2006) sequence, proves an attractive solution within the boundaries of the formal scenario. We calculated the magnitude of the K-correction at this mass ratio using our irradiated secondary model. In order to produce the observed $K_{em} = 82.2 \pm 4.9$ km s^{-1}, we find a true $K_2 = 100.8 \pm 7.1$ km s^{-1} where the error is calculated by propagating the error on K_{em}. This error dominates over effects such as the assumed level of equatorial shielding or the optical thickness of the emission. The implied system parameters based on this assumed q and calculated K_2 can be found in the left hand column of Table 5.

The small mass ratio scenario would correspond to a low mass donor with a M8 (Cox 2000) or T spectral type (Knigge 2006) if the donor is close to its main-sequence configuration. This would agree with the infrared magnitude constraints mentioned previously and fits perfectly with GW Lib being close to the period minimum.

Interestingly, the derived K_1 in this scenario is close to the measured radial velocity of the narrow Balmer emission component in outburst ($K = 3.0 \pm 1.6$ km s^{-1}) suggesting that this component may trace the WD when irradiated by the accretion disc. Similar sharp emission components from the WD are seen in AM CVn systems (Morales-Rueda et al. 2003, Roelofs et al. 2006). However, a component arising at the surface of a WD is expected to be gravitationally red-shifted but the systemic velocity for this lines component was -16.6 ± 0.8 km s^{-1} which is similar to the systemic velocity of the system and cannot be biased by the Stark effect as is the case in AM CVn systems. Unfortunately the emission is only a transient feature and the constraint on its K will be difficult to improve upon. The origin of the component and its possible connection with the WD thus remains unclear.

6 DISCUSSION

We presented time-resolved optical spectroscopy of GW lib during a large number of epochs spanning before, throughout and after the 2007 outburst. We studied the long-term evolution of the spectral features tracking large changes in the accretion geometry and intensity.

Pre-outburst spectroscopy obtained in 2004 data show clear features of the accreting WD including a detection of Mg II absorption. Here, the low inclination of GW Lib has the advantage over high inclination system as it gives narrow disc emission lines instead of wide profiles, potentially resolving the line from the nearby He I line. Higher resolution, high signal to noise spectra around this line in quiescence could provide a dynamical trace of the accreting WD and give a directly measured mass constraint to complement the constraints indirectly obtained from seismology.

During the outburst, we initially see the optically thick accretion disc dominate through broad absorption features. Their radial velocity does not trace the WD and show semi-amplitudes of order 50 km/s. A peculiar sharp emission line component was found in the Balmer lines that is effectively stationary. This could be some low velocity outflow in the z-direction or a component near the WD, but its mean velocity is similar to γ whereas a layer near the high gravity WD should be gravitationally red-shifted. As the system fades back towards quiescence, accretion powered double-peaked emission profiles appear. The absorption associated with the accretion disc continues to weaken until the system returns to a semi-quiescent state with strong double-peaked emission lines.

The Ca II triplet in GW Lib shows that these much neglected lines of CV spectra could be an interesting window to search for signs of both donor stars and accretion disc structures even in cases where the Balmer lines show no signs of the donor star whatsoever and the disc itself is barely resolved. GW Lib is a particularly challenging object in that sense due its very low inclination and thus small projected velocities. The Ca II triplet in emission could be resolved into several components and the secondary star was discovered in emission moving in between the sharp double-peaked emission from the accretion disc. Doppler tomography and radial velocity profiles fits of the Ca II lines provide a semi-amplitude of $K_{em} = 82.2 \pm 4.9$ km s^{-1} for this donor star feature and indicates a disc centre of symmetry at $K_{disc} = 6 \pm 5$ km s^{-1}. The disc is also visible in the Hβ maps but with less detail and sharpness and no donor star contribution is seen. Contrasting these lines highlights the diagnostic advantages provided by the Ca II triplet.

Based on previous studies together with the limits on K_1 and K_2 provided in this work, the allowed range of binary parameters were explored. While our dynamical limits place a hard upper limit on the binary mass ratio of $q < 0.23$, we favour a significantly lower value. A mass ratio near $q \sim 0.06$ is in accordance with estimates based on the detected super-hump modulations, the constraints on the faintness, and thus mass, of the donor star and the indications that K_1 is very small. Given such a mass ratio, our measured K_{em} implies $K_2 = 100.8 \pm 7.1$ km s^{-1} for the donor star component when applying the relevant K-correction. The implied $K_1 = 6.2 \pm 0.4$ km s^{-1} is then also close to our measured disc centre of symmetry. The combination of a

WD mass near the value suggested by the pulsations and a low mass donor near the empirical sequence of an evolved CV near the period bounce appears to be consistent with the observational constraints to date.

Whether the spectral features observed several months after the tail end of the 2007 outburst are persistent remains to be established. As the WD continues to cool, donor star irradiation may be less effective in exciting the strong Ca II lines we observed. Nonetheless, high resolution spectroscopy resolving these lines at good S/N levels appears to be a viable tool to expand our knowledge of the binary parameters of short period cataclysmic variables and their faint donor stars.

ACKNOWLEDGMENTS

REFERENCES

Araujo-Betancor S., Gänsicke B.T., Hagen H.-J. et al., 2005, A&A, 430, 629A

Bigelow B. C., Dressler A., 2003, Proc. SPIE, 4841, 1727

Cox A.N., 2000, Allen's Astrophysical Quantities, Springer-Verlag New York Inc., 4Rev Ed edition

Copperwheat C.M., Marsh T.R., Dhillon V.S. et al., 2009, MNRAS, 393, 157

Duerbeck H.W. & Seitter W.C., 1987, AP &SS, 131, 467

Fabricant D.G., Cheimets P., Caldwell N., Geary J., PASP, 1998, 110, 79

González L.E. & Maza J., 1983, IAU Circ, 3854

Gänsicke B.T., Dillon M., Southworth J. et al., 2009, MNRAS, 2009arXiv0905.3476G

Groot P., 2001, ApJ, 551, 89

Hessman F.V., Robinson E.L., Nather R. E., Zhang, E.-H., 1984, ApJ, 286, 747

Hiroi, K., Nogami, D., Ueda Y. et al., 2009, PASJ, 2009arXiv0904.3425H

Horne K., 1986, PASP, 98. 609

Horne K., 1995, A&A, 297, 273

Kafka, S., Honeycutt, R.K., 2006, AJ, 132, 1517

Kato T., Maehara H. & Monard B., 2008, PASJ, 60, 23K

Knigge C., 2006, MNRAS, 374, 484

Kolb, U., Ritter, H., 1992, A&A, 254, 213

Littlefair S.P., Dhillon V.S., Marsh T.R., G änsicke B.T., Southworth J., Watson C.A., 2006. Sci, 314, 1578

Littlefair S.P., Dhillon V.S., Marsh T.R., G änsicke B.T., Southworth, J., Baraffe I., Watson, C.A., Copperwheat C., 2008, MNRAS, 388, 1582

Long, K.S., Sion E.M., Gänsicke B.T., Szkody P., 2004, ApJ, 602, 948

North R.C., Marsh T.R., Kolb U., Dhillon V.S., Moran C.K.J., 2002, MNRAS, 337, 1215

Marsh T.R., 1989, PASP, 101, 1032

Marsh T.R., 2001, Astrotomography, Indirect Imaging Methods in Observational Astronomy, LNP 573, 1, Springer-Verslag Berlin, Edited by H.M.J Boffin, D. Steegs, J. Cuypers

Marsh T.R., Dhillon V.S., 1997, MNRAS, 292, 385

Mennickent, R. E., Unda-Sanzana, E., Tappert, C., 2006, A&A, 451, 613

Morales-Rueda L., Marsh T.R., Steeghs D., Unda-Sanzana E., Wood J.H., North R.C., 2003, A&A, 405, 249

Neilsen, J., Steeghs, D., Vrtilek, S. D., 2008, MNRAS, 384, 849

Osterbrock D.E., Ferland G.J., 2006, Astrophysics of Gaseous Nebulae and Active Galactic Nuclei, second edition, University Science Books, Causalito, California 1982, AJ, 254, 616

Rappaport, S.A., Verbunt, F., & Joss, P.C., 1983, ApJ, 275, 713

Patterson, J., Fenton W.H., Thorstensen J.R. et al., 2002, PASP, 114, 721P

Patterson, J., Kemp J., Harvey D.A. et al., 2005, PASP, 117, 1204

Ritter H., Kolb U. 2003, A&A, 404, 301 (update RKcat7.11, 2009)

Roelofs G.H.A., Groot P.J., Nelemans G., Marsh T.R., Steeghs D., 2006, MNRAS, 371, 1231

Schneider D.P. & Young P., 1980, ApJ, 238, 946

Steeghs D., Horne K., Marsh T.R., Donati J.F., 1996, MNRAS, 281, 626

Steeghs, D., Harlaftis E.T. & Horne, K., 1997, MNRAS, 290

Steeghs D. & Casares J., 2002, ApJ, 568, 273

Southworth, J., Marsh T.R., Gänsicke B.T., Aungwerojwit A., Hakala P., de Martino D., Lehto H., 2007, MNRAS, 382, 1145

Szkody P., Desai V., Hoard D.W., 2000, AJ, 119, 365

Szkody P., Gänsicke B.T., Howell S.B., Sion E.M., ApJ, 2002, 575, L79

Thortensen J.R., Patterson J., Kemp J., Vennes S., 2002, PASP, 114, 1108

Thortensen J.R, 2003, AJ, 126, 3017

Tokarz S.P., Roll J., 1997, ASPC, 125, 140

Townsley D.M., Arras P., Bildsten L., 2004, AJ, 609, 105

Templeton M. R., 2007, AAN, 349, 1T

Wade R.A. & Horne K., 1988, ApJ, 324, 411

Warner B., 1995, Cataclysmic Variable Stars. Cambridge Astrophysics Series. Cambridge Univ. Press, Cambridge

van Zyl L., Warner B., O'Donoghue D., Sullivan D., Pritchard J., Kemp J., 2000, Baltic Astr., 9, 231

van Zyl L., Warner B., O'Donoghue D. et al., 2004, MNRAS, 350, 307